WAVE PROPAGATION, LOCALIZATION AND DISPERSION IN A GRADIENT-DEPENDENT MEDIUM

L. J. SLUYS

Delft University of Technology, Department of Civil Engineering, P.O. Box 5048,
2600 GA Delft, Netherlands

R. DE BORST

Delft University of Technology, Department of Civil Engineering/TNO Building and Construction
Research, P.O. Box 5048, 2600 GA Delft, Netherlands

and

H.-B. MÜHLHAUS

CSIRO Division of Geomechanics, P.O. Box 54, Mt. Waverley, Victoria 3149, Australia

Abstract—A continuum model that incorporates a dependence upon the Laplacian of the inelastic strain is used to regularize the initial value problem that results from the introduction of strain softening or non-associated flow. It is shown that the introduction of this gradient dependence preserves well-posedness of the initial value problem and that wave propagation in the enhanced continuum is dispersive. An analysis of the dispersive wave propagation reveals the existence of an internal length scale. Numerical analyses of one-dimensional and two-dimensional problems confirm that this internal length scale sets the localization zone and show that the results are insensitive to the fineness of the discretization and to the direction of the grid lines. This holds true with respect to the strain profiles, the energy dissipation and the extent of wave reflection.

1. INTRODUCTION

Micro-structural phenomena such as micro-cracking and void or pore nucleation and growth, which occur in a localization zone, cause discontinuous deformation processes which cannot be described with classical continuum models. Therefore, various kinds of modifications and generalizations of standard continuum plasticity have been proposed to avoid a spurious solution for the localization zone and an excessive mesh dependence. One type of enrichment is based on the inclusion of higher-order spatial derivatives in the constitutive equations (Aifantis, 1984; Schreyer and Chen, 1986; Lasry and Belytschko, 1988; Zbib and Aifantis, 1988; Mühlhaus and Aifantis, 1991; de Borst and Mühlhaus, 1991, 1992; Aifantis, 1992) or the averaging of strains, the so-called non-local models (Bažant *et al.*, 1984; Pijaudier-Cabot and Bažant, 1987). In the approach followed in this paper we include the second-order strain gradient terms in the stress–strain law. Mühlhaus and Aifantis (1991) and de Borst and Mühlhaus (1991) have shown that such a gradient-dependent model can be derived from non-local models. Gradient models as well as non-local models reflect the fact that the interaction between micro-structural deformations in the localization zone is non-local.

The use of a higher-order gradient model can result in a well-posed set of partial differential equations. From a dispersion analysis it becomes clear that the wave speeds remain real under strain-softening conditions and that the continuum is capable of transforming a travelling wave into a stationary localization wave. Furthermore, the analysis of dispersive wave propagation reveals the existence of an internal length scale. As a consequence of the well-posedness of the mathematical problem numerical results do not suffer from a pathological mesh dependence.

The paper is organized as follows. First, a description is given of the gradient model, in which the yield function not only depends on the stress and a hardening/softening parameter, but also on the Laplacian of the latter quantity. We investigate wave propagation in a bar of gradient-dependent material by means of a dispersion analysis. This study leads

to an exact prediction of the width of the localization zone. Next, the algorithmic difficulties caused by the incorporation of the gradient effect are discussed. Results of numerical analyses are presented for a uniaxial bar problem in tension (mode-I localization problem) and an impact biaxial test (mode-II localization problem).

2. FORMULATION OF A GRADIENT-DEPENDENT PLASTICITY MODEL

The framework of the gradient-dependent continuum is set by the following equations:

$$\mathbf{L}^{\mathrm{T}}\boldsymbol{\sigma} = \mathbf{R}\ddot{\mathbf{u}}, \tag{1}$$

$$\boldsymbol{\varepsilon} = \mathbf{L}\mathbf{u}, \tag{2}$$

$$\dot{\boldsymbol{\sigma}} = \mathbf{D}_{\mathrm{e}}(\dot{\boldsymbol{\varepsilon}} - \dot{\boldsymbol{\varepsilon}}_{\mathrm{p}}), \tag{3}$$

$$\dot{\boldsymbol{\varepsilon}}_{\mathrm{p}} = \dot{\lambda}\mathbf{m}, \quad \dot{\lambda} \geqslant 0, \tag{4}$$

$$f(\boldsymbol{\sigma}, \kappa, \nabla^2\kappa) \leqslant 0, \quad f\dot{\lambda} = 0. \tag{5}$$

In the equation of motion (1) $\boldsymbol{\sigma}$ is a vector containing the stress components (σ_{xx}, σ_{yy}, σ_{zz}, σ_{xy}, σ_{yz}, σ_{zx}) and in the vector $\mathbf{u}$ the displacement components are assembled (u_x, u_y, u_z). A superimposed dot denotes differentiation with respect to time and a superimposed double dot implies that a quantity is differentiated twice, which means that $\ddot{\mathbf{u}}$ is the acceleration vector. The density matrix $\mathbf{R}$ is equal to diag$[\rho, \rho, \rho]$ with density ρ. In (1) and (2) the differential operator matrix $\mathbf{L}$ is defined as

$$\mathbf{L}^{\mathrm{T}} = \begin{bmatrix} \dfrac{\partial \cdot}{\partial x} & 0 & 0 & \dfrac{\partial \cdot}{\partial y} & 0 & \dfrac{\partial \cdot}{\partial z} \\[2mm] 0 & \dfrac{\partial \cdot}{\partial y} & 0 & \dfrac{\partial \cdot}{\partial x} & \dfrac{\partial \cdot}{\partial z} & 0 \\[2mm] 0 & 0 & \dfrac{\partial \cdot}{\partial z} & 0 & \dfrac{\partial \cdot}{\partial y} & \dfrac{\partial \cdot}{\partial x} \end{bmatrix}, \tag{6}$$

and the superscript T is the transpose symbol. In the kinematic equation (2) the relations are given between the strain components (ε_{xx}, ε_{yy}, ε_{zz}, $2\varepsilon_{xy}$, $2\varepsilon_{yz}$, $2\varepsilon_{zx}$), assembled in the vector $\boldsymbol{\varepsilon}$ and the displacement components. We also introduce the vector $\boldsymbol{\varepsilon}^*$ of the unweighted tensor components, so that $\boldsymbol{\varepsilon}^{\mathrm{T}}\boldsymbol{\varepsilon}^* = \varepsilon_{ij}\varepsilon_{ij}$. In the constitutive equations (3)–(5) the matrix $\mathbf{D}_{\mathrm{e}}$ contains the elastic stiffness moduli and $\dot{\lambda}$ is a non-negative scalar, which represents the magnitude of the plastic strain rate $\dot{\boldsymbol{\varepsilon}}_{\mathrm{p}}$. The vector $\mathbf{m}$ denotes the direction of the plastic flow in the stress space and is defined as the gradient of the plastic potential function g:

$$\mathbf{m} = \frac{\partial g}{\partial \boldsymbol{\sigma}}. \tag{7}$$

In the gradient-plasticity model considered here, the yield strength depends not only upon the equivalent plastic strain κ, but also upon the Laplacian thereof. As in conventional plasticity, the stress point must remain on the yield surface during plastic deformation, which gives the consistency condition for continuing plastic flow:

$$\frac{\partial f^{\mathrm{T}}}{\partial \boldsymbol{\sigma}}\dot{\boldsymbol{\sigma}} + \frac{\partial f}{\partial \kappa}\dot{\kappa} + \frac{\partial f}{\partial \nabla^2\kappa}\nabla^2\dot{\kappa} = 0. \tag{8}$$

If we use the gradient to the yield surface $\mathbf{n}$ according to

$$\mathbf{n} = \frac{\partial f}{\partial \boldsymbol{\sigma}}, \tag{9}$$

and the hardening/softening modulus h as defined in conventional plasticity:

$$h = -\frac{1}{\lambda} \frac{\partial f}{\partial \kappa} \dot{\kappa}, \tag{10}$$

and assume the dependence of f upon $\nabla^2 \kappa$ to be a constant:

$$\bar{c} = \frac{\partial f}{\partial \nabla^2 \kappa}, \tag{11}$$

the consistency equation can be rewritten as

$$\mathbf{n}^T \dot{\boldsymbol{\sigma}} - h\dot{\lambda} + \bar{c}\nabla^2 \dot{\kappa} = 0. \tag{12}$$

Furthermore, it is assumed that

$$\dot{\kappa} = \eta\dot{\lambda}, \tag{13}$$

with η a constant. The latter represents a certain limitation of the model but large classes of hardening/softening hypotheses and yield functions in fact satisfy eqn (13). In this paper we apply the strain-hardening/softening hypothesis as defined by

$$\dot{\kappa} = \sqrt{\tfrac{2}{3}(\dot{\boldsymbol{\varepsilon}}_p)^T \dot{\boldsymbol{\varepsilon}}_p^*}. \tag{14}$$

Combined with the yield criteria:

$$f(\boldsymbol{\sigma}, \kappa, \nabla^2 \kappa) = \sqrt{3J_2} - \bar{\sigma}(\kappa, \nabla^2 \kappa), \tag{15}$$

for von Mises, with the second invariant $J_2 = \tfrac{1}{2}(s_1^2 + s_2^2 + s_3^2)$ and s_i the deviatoric stresses:

$$f(\boldsymbol{\sigma}, \kappa, \nabla^2 \kappa) = \sqrt{3J_2} + \alpha p - \bar{\sigma}(\kappa, \nabla^2 \kappa), \tag{16}$$

for Drucker–Prager, with p the hydrostatic pressure, α a friction coefficient and $\bar{\sigma}$ reflecting the cohesion of the material, and

$$f(\boldsymbol{\sigma}, \kappa, \nabla^2 \kappa) = \sigma_i - \bar{\sigma}(\kappa, \nabla^2 \kappa), \tag{17}$$

for Rankine, with $\sigma_i = \max(\sigma_1, \sigma_2, \sigma_3)$, we obtain

$$\eta = 1 \quad \text{for von Mises and Rankine} \tag{18}$$

and

$$\eta = \sqrt{1 + \tfrac{2}{9}\alpha^2} \quad \text{for Drucker–Prager.} \tag{19}$$

If we use $\bar{c}_\eta = \eta\bar{c}$ eqn (12) can be written as

$$\mathbf{n}^T \dot{\boldsymbol{\sigma}} - h\dot{\lambda} + \bar{c}_\eta \nabla^2 \dot{\lambda} = 0. \tag{20}$$

So, for gradient-dependent plasticity, the consistency condition results in a differential equation for $\dot{\lambda}$ and an explicit expression for $\dot{\lambda}$ in terms of $\dot{\boldsymbol{\varepsilon}}$ at a local (integration point) level, as in conventional plasticity, cannot be obtained.

3. WAVE PROPAGATION IN A ONE-DIMENSIONAL GRADIENT-DEPENDENT BAR

To demonstrate the salient features of our model we consider a one-dimensional situation for which the governing equations of motion [*cf.* eqn (1)], the kinematic equation [*cf.* eqn (2)] and the constitutive equation [*cf.* eqn (5)] can be written in rate form:

$$\frac{\partial \dot{\sigma}}{\partial x} = \rho \frac{\partial^2 v}{\partial t^2}, \tag{21}$$

$$\dot{\varepsilon} = \frac{\partial v}{\partial x}, \tag{22}$$

$$\dot{\sigma} = h\dot{\varepsilon}_p - \bar{c}\frac{\partial^2 \dot{\varepsilon}_p}{\partial x^2}, \tag{23}$$

respectively, in which velocity $v = \dot{u}$, the equivalent plastic strain rate $\dot{\kappa}$ equals the axial plastic strain rate $\dot{\varepsilon}_p$ and a linear strain-softening function is utilized ($h = $ const.). Combining eqns (21), (22) and (23), and taking $\dot{\varepsilon}_p = \dot{\varepsilon} - \dot{\varepsilon}_e$ and $\dot{\varepsilon}_e = \dot{\sigma}/E$, we can obtain the wave equation for a one-dimensional gradient-dependent, strain-softening bar:

$$\bar{c}\left(\frac{\partial^4 v}{\partial x^4} - \frac{1}{c_e^2}\frac{\partial^4 v}{\partial x^2 \partial t^2}\right) + \frac{E+h}{c_e^2}\frac{\partial^2 v}{\partial t^2} - h\frac{\partial^2 v}{\partial x^2} = 0, \tag{24}$$

in which $c_e = \sqrt{E/\rho}$. If $\bar{c} \to 0$ the wave equation for a classical strain-softening bar is recovered with imaginary characteristics and imaginary wave speeds (Sluys, 1992). Equation (24) can be investigated by means of its characteristics. To this end we consider the variation of two third-order derivative terms of the velocity v, namely

$$d\left(\frac{\partial^3 v}{\partial x^3}\right) = \frac{\partial^4 v}{\partial x^3 \partial t}dt + \frac{\partial^4 v}{\partial x^4}dx \tag{25}$$

and

$$d\left(\frac{\partial^3 v}{\partial x^2 \partial t}\right) = \frac{\partial^4 v}{\partial x^2 \partial t^2}dt + \frac{\partial^4 v}{\partial x^3 \partial t}dx. \tag{26}$$

The combination of eqns (25) and (26) and the wave equation for the gradient-dependent bar (24) yields a system of three fourth-order differential equations with a characteristic determinant:

$$D = \begin{bmatrix} \bar{c} & 0 & -\bar{c}/c_e^2 \\ dx & dt & 0 \\ 0 & dx & dt \end{bmatrix} = \bar{c}(dt^2 - (1/c_e^2)dx^2). \tag{27}$$

With $D = 0$ the characteristics are equal to the elastic bar velocity $\pm c_e$ and remain real when strain softening occurs. So, the wave equation remains hyperbolic and the initial value problem is well-posed.

We now carry out a dispersion analysis for the gradient-dependent bar. We consider the general solution for a single harmonic wave propagating through a one-dimensional continuum with a velocity field of the form:

$$v(x, t) = A e^{i(kx - \omega t)}, \tag{28}$$

in which ω is the angular frequency and k is the wave number counting the number of wave lengths λ in the bar over 2π:
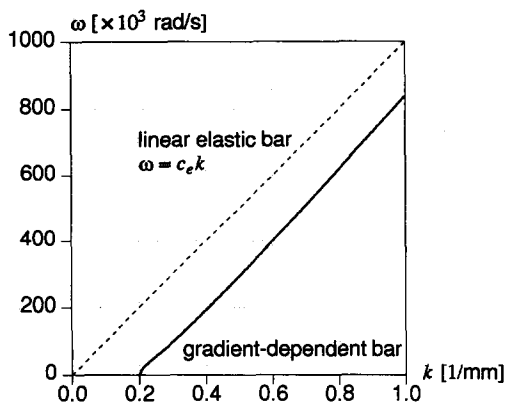
Fig. 1. Dispersion relation for the gradient-dependent bar.

$$k = \frac{2\pi}{\lambda}. \tag{29}$$

Substitution of eqn (28) into the wave equation (24) gives the dispersion relation for the gradient-dependent bar:

$$\bar{c}k^4 - (\bar{c}/c_e^2)k^2\omega^2 - ((E+h)/c_e^2)\omega^2 + hk^2 = 0. \tag{30}$$

We consider the positive root for ω:

$$\omega = c_e\sqrt{\frac{h+\bar{c}k^2}{E+h+\bar{c}k^2}}k, \tag{31}$$

and recover the non-dispersive equation for the classical strain-softening bar when $\bar{c} \to 0$ (Sluys, 1992). The dispersion relation (31) is plotted in Fig. 1 for the data set of the one-dimensional bar problem, treated in Section 5.1. The phase velocity $c_f = \omega/k$ of the harmonic wave reads:

$$c_f = c_e\sqrt{\frac{h+\bar{c}k^2}{E+h+\bar{c}k^2}}. \tag{32}$$

Equation (32) is plotted in Fig. 2. The phase speed c_f depends on the wave number k and, consequently, wave propagation is dispersive (Whitham, 1974) for the gradient-dependent
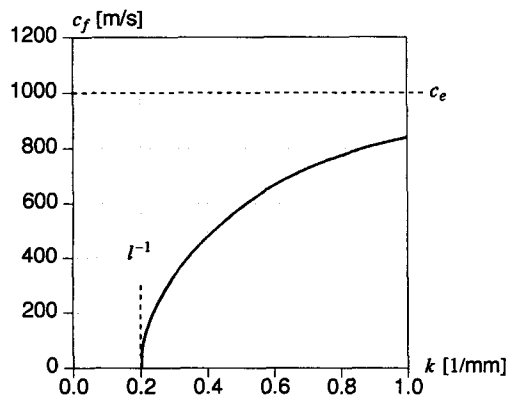

Fig. 2. Phase velocity–wave number curve for the gradient-dependent bar.

bar. Owing to the fact that different harmonic waves propagate with different velocities the shape of a pulse is altered and a loading wave can be transformed into a stationary localization wave in the gradient-dependent medium. From eqn (32) it follows that the phase velocity remains real if

$$k \geqslant \sqrt{-\frac{h}{\bar{c}}} \quad \text{and thus } \lambda \leqslant 2\pi l, \quad \text{with } l = \sqrt{-\frac{\bar{c}}{h}}. \tag{33}$$

Thus for a gradient-dependent model the phase speed does not necessarily become imaginary at the onset of softening, as in a classical model. The parameter l is now the internal length scale in the gradient-dependent model. If $k < l^{-1}$ or the wave length $\lambda > 2\pi l$, we recover the situation in which a disturbance δv is unbounded and stability in the sense of Lyapunov is lost (i.e. a small disturbance of boundary data results in large changes of the response). However, strain-softening regions remain small and no wave lengths larger than $2\pi l$ can occur because they do not fit within the strain-softening region. Consequently, all phase velocities remain real, because the first-order wave with the lowest wave number (or largest wave length) has a wave number which is larger than the critical value in eqn (33). In the numerical analyses in Section 5 we will see that all higher frequencies which are present in a loading wave vanish under the influence of material damping and we obtain a stationary harmonic localization wave with a width w equal to the maximum wave length $\lambda = 2\pi l$.

4. ALGORITHMIC ASPECTS

While eqns (1) and (20) describe the equation of motion and the evolution of the elasto-plastic process in a strong sense a weak form of these equations is obtained by setting:

$$\int_V \delta \mathbf{u}^{\mathrm{T}} [\mathbf{L}^{\mathrm{T}} \boldsymbol{\sigma} - \mathbf{R}\ddot{\mathbf{u}}] \, \mathrm{d}V = 0 \tag{34}$$

and

$$\int_V \delta \lambda \, f(\boldsymbol{\sigma}, \kappa, \nabla^2 \kappa) \, \mathrm{d}V = 0, \tag{35}$$

in which δ denotes the variation of a quantity. Using Green's theorem:

$$\int_V \delta \mathbf{u}^{\mathrm{T}} [\mathbf{L}^{\mathrm{T}} \boldsymbol{\sigma}] \, \mathrm{d}V = -\int_V \delta \boldsymbol{\varepsilon}^{\mathrm{T}} \boldsymbol{\sigma} \, \mathrm{d}V + \int_S \delta \mathbf{u}^{\mathrm{T}} \mathbf{t} \, \mathrm{d}S, \tag{36}$$

eqn (34) becomes

$$\int_V \delta \mathbf{u}^{\mathrm{T}} [\mathbf{R}\ddot{\mathbf{u}}] \, \mathrm{d}V + \int_V \delta \boldsymbol{\varepsilon}^{\mathrm{T}} \boldsymbol{\sigma} \, \mathrm{d}V = \int_S \delta \mathbf{u}^{\mathrm{T}} \mathbf{t} \, \mathrm{d}S. \tag{37}$$

If eqn (37) is considered to be valid at time $t + \Delta t$ the evolution of the stress history follows from

$$\boldsymbol{\sigma}^{t+\Delta t} = \boldsymbol{\sigma}^t + \int_t^{t+\Delta t} \dot{\boldsymbol{\sigma}} \, \mathrm{d}\tau. \tag{38}$$

Substitution into eqn (37) yields:

$$\int_V \delta \mathbf{u}^{\mathrm{T}} [\mathbf{R} \ddot{\mathbf{u}}^{t+\Delta t}] \, dV + \int_V \delta \boldsymbol{\varepsilon}^{\mathrm{T}} \int_t^{t+\Delta t} \dot{\boldsymbol{\sigma}} \, d\tau \, dV = \int_S \delta \mathbf{u}^{\mathrm{T}} \mathbf{t}^{t+\Delta t} \, dS - \int_V \delta \boldsymbol{\varepsilon}^{\mathrm{T}} \boldsymbol{\sigma}^t \, dV. \qquad (39)$$

The yield function at $t + \Delta t$ can be written as

$$f(\boldsymbol{\sigma}^{t+\Delta t}, \kappa^{t+\Delta t}, \nabla^2 \kappa^{t+\Delta t}) = f(\boldsymbol{\sigma}^t, \kappa^t, \nabla^2 \kappa^t) + \int_t^{t+\Delta t} \dot{f}(\boldsymbol{\sigma}, \kappa, \nabla^2 \kappa) \, d\tau. \qquad (40)$$

With the consistency equation (20) and eqn (40), eqn (35) can now be modified to

$$\int_V \delta \lambda \int_t^{t+\Delta t} [\mathbf{n}^{\mathrm{T}} \dot{\boldsymbol{\sigma}} - h\dot{\lambda} + \bar{c}_\eta \nabla^2 \dot{\lambda}] \, d\tau \, dV = - \int_V \delta \lambda f(\boldsymbol{\sigma}^t, \kappa^t, \nabla^2 \kappa^t) \, dV. \qquad (41)$$

Substitution of eqn (4) into eqn (3) gives

$$\dot{\boldsymbol{\sigma}} = \mathbf{D}_e (\dot{\boldsymbol{\varepsilon}} - \dot{\lambda} \mathbf{m}). \qquad (42)$$

If we substitute this relationship in eqns (39) and (41) we obtain

$$\int_V \delta \mathbf{u}^{\mathrm{T}} [\mathbf{R} \ddot{\mathbf{u}}^{t+\Delta t}] \, dV + \int_V \delta \boldsymbol{\varepsilon}^{\mathrm{T}} \int_t^{t+\Delta t} \mathbf{D}_e (\dot{\boldsymbol{\varepsilon}} - \dot{\lambda} \mathbf{m}) \, d\tau \, dV = \int_S \delta \mathbf{u}^{\mathrm{T}} \mathbf{t}^{t+\Delta t} \, dS - \int_V \delta \boldsymbol{\varepsilon}^{\mathrm{T}} \boldsymbol{\sigma}^t \, dV = 0 \qquad (43)$$

and

$$\int_V \delta \lambda \int_t^{t+\Delta t} [\mathbf{n}^{\mathrm{T}} \mathbf{D}_e \dot{\boldsymbol{\varepsilon}} - (h + \mathbf{n}^{\mathrm{T}} \mathbf{D}_e \mathbf{m}) \dot{\lambda} + \bar{c}_\eta \nabla^2 \dot{\lambda}] \, d\tau \, dV = - \int_V \delta \lambda f(\boldsymbol{\sigma}^t, \kappa^t, \nabla^2 \kappa^t) \, dV. \qquad (44)$$

It should be mentioned that in contrast to the conventional approach in computational plasticity, the plastic multiplier is taken as an independent variable. While this approach is, in principle, also possible in gradient-independent plasticity, it does not seem to entail major advantages when compared with return-mapping algorithms (Ortiz and Simo, 1986; de Borst and Feenstra, 1990). For gradient plasticity, i.e. when $\bar{c}_\eta \neq 0$ in eqn (44), however, the discretization of λ seems natural and automatically satisfies the consistency condition in a distributed sense (Simo, 1989). Other alternatives of dealing with the extra partial differential equation have been discussed by de Borst and Mühlhaus (1991).

We will now discuss the spatial discretization of the problem. The body can be divided into a finite number of elements and for each element the continuous displacement field $\mathbf{u}$ can be interpolated by

$$\mathbf{u} = \mathbf{H} \mathbf{a}, \qquad (45)$$

and the continuous acceleration field by

$$\ddot{\mathbf{u}} = \mathbf{H} \ddot{\mathbf{a}}, \qquad (46)$$

in which the matrix $\mathbf{H}$ contains the interpolation polynomials and $\mathbf{a}$ and $\ddot{\mathbf{a}}$ the nodal displacements and nodal accelerations, respectively. Combining eqns (2) and (45) and introducing the strain-nodal displacement matrix:

$$\mathbf{B} = \mathbf{L} \mathbf{H}, \qquad (47)$$

the relation between the strains and the nodal displacements is obtained as

$$\varepsilon = \mathbf{B}\mathbf{a}, \tag{48}$$

or in rate format as

$$\dot{\varepsilon} = \mathbf{B}\dot{\mathbf{a}}. \tag{49}$$

We can discretize the plastic multiplier λ in a similar fashion by

$$\lambda = \mathbf{h}^{\mathrm{T}}\mathbf{\Lambda}, \tag{50}$$

with vector $\mathbf{h}$ containing the shape functions $h_1, \ldots, h_n$ for the interpolation of the plastic multiplier and $\mathbf{\Lambda}$ denoting the vector of additional nodal degrees-of-freedom. Equation (50) in a rate form yields

$$\dot{\lambda} = \mathbf{h}^{\mathrm{T}}\dot{\mathbf{\Lambda}}. \tag{51}$$

Since the Laplacian operator of $\dot{\lambda}$ must also be computed, the differential operator vector $\mathbf{p}$ is introduced:

$$\nabla^2\dot{\lambda} = \mathbf{p}^{\mathrm{T}}\dot{\mathbf{\Lambda}}, \tag{52}$$

in which $\mathbf{p}$ is defined by

$$\mathbf{p} = [\nabla^2 h_1, \ldots, \nabla^2 h_n]^{\mathrm{T}}. \tag{53}$$

Generally, the vector $\mathbf{h}$ will not contain the same interpolation polynomials as $\mathbf{H}$. While the interpolation of the displacement degrees-of-freedom requires only C^0-continuity, the fact that second derivatives of $\dot{\lambda}$ enter the weak form of the consistency condition makes it necessary to select C^1-continuous shape functions for the interpolation of $\dot{\lambda}$. For instance, for the one-dimensional examples that will be treated in a subsequent section, a Hermitian interpolation is employed for $\dot{\lambda}$ and linear interpolation is used for u_x, quite similar to beam-column elements where the interpolation of the transverse displacements is usually also achieved through Hermitian shape functions and the axial displacements are interpolated linearly.

Next we substitute eqns (45), (46), (48), (49), (50), (51) and (52) into eqns (43) and (44). The result is

$$\delta\mathbf{a}^{\mathrm{T}}\int_V \mathbf{H}^{\mathrm{T}}\mathbf{R}\mathbf{H}\ddot{\mathbf{a}}^{t+\Delta t} + \delta\mathbf{a}^{\mathrm{T}}\int_V\int_t^{t+\Delta t}[\mathbf{B}^{\mathrm{T}}\mathbf{D}_e\mathbf{B}\dot{\mathbf{a}} - \mathbf{B}^{\mathrm{T}}\mathbf{D}_e\mathbf{m}\mathbf{h}^{\mathrm{T}}\dot{\mathbf{\Lambda}}]\,\mathrm{d}\tau\,\mathrm{d}V$$

$$= \delta\mathbf{a}^{\mathrm{T}}\int_S \mathbf{H}^{\mathrm{T}}\mathbf{t}^{t+\Delta t}\,\mathrm{d}S - \delta\mathbf{a}^{\mathrm{T}}\int_V \mathbf{B}^{\mathrm{T}}\mathbf{\sigma}^t\,\mathrm{d}V \quad (54)$$

and

$$\delta\mathbf{\Lambda}^{\mathrm{T}}\int_V\int_t^{t+\Delta t}[-\mathbf{h}\mathbf{n}^{\mathrm{T}}\mathbf{D}_e\mathbf{B}\dot{\mathbf{a}} + (h + \mathbf{n}^{\mathrm{T}}\mathbf{D}_e\mathbf{m})\mathbf{h}\mathbf{h}^{\mathrm{T}}\dot{\mathbf{\Lambda}} - \bar{c}_{\eta}\mathbf{h}\mathbf{p}^{\mathrm{T}}\dot{\mathbf{\Lambda}}]\,\mathrm{d}\tau\,\mathrm{d}V$$

$$= \delta\mathbf{\Lambda}^{\mathrm{T}}\int_V f(\mathbf{\sigma}^t, \kappa^t, \nabla^2\kappa^t)\mathbf{h}\,\mathrm{d}V. \quad (55)$$

We assume Euler forward predictions for the time integrals in eqns (54) and (55). Therefore in the zeroth iteration of a Newton–Raphson scheme we take $\mathbf{n}$, $\mathbf{m}$ and h at time t. We define the incremental nodal displacement vector as

$$\Delta \mathbf{a} = \int_t^{t+\Delta t} \dot{\mathbf{a}} \, \mathrm{d}\tau \tag{56}$$

and the incremental plastic multiplier as

$$\Delta \Lambda = \int_t^{t+\Delta t} \dot{\Lambda} \, \mathrm{d}\tau. \tag{57}$$

Substitution of eqns (56) and (57) into eqns (54) and (55) and assuming that the identities (54) and (55) must hold for any admissible $\delta \mathbf{a}$ and $\delta \Lambda$ the following set of algebraic equations ensues:

$$\int_V \mathbf{H}^T \mathbf{R} \mathbf{H} \ddot{\mathbf{a}}^{t+\Delta t} \, \mathrm{d}V + \int_V [\mathbf{B}^T \mathbf{D}_e \mathbf{B} \Delta \mathbf{a} - \mathbf{B}^T \mathbf{D}_e \mathbf{m}' \mathbf{h}^T \Delta \Lambda] \, \mathrm{d}V = \int_S \mathbf{H}^T \mathbf{t}^{t+\Delta t} \, \mathrm{d}S - \int_V \mathbf{B}^T \boldsymbol{\sigma}^t \, \mathrm{d}V \tag{58}$$

and

$$\int_V [-\mathbf{h}(\mathbf{n}')^T \mathbf{D}_e \mathbf{B} \Delta \mathbf{a} + (h' + (\mathbf{n}')^T \mathbf{D}_e \mathbf{m}') \mathbf{h} \mathbf{h}^T \Delta \Lambda - \bar{c}_\eta \mathbf{h} \mathbf{p}^T \Delta \Lambda] \, \mathrm{d}V = \int_V f(\boldsymbol{\sigma}^t, \kappa^t, \nabla^2 \kappa^t) \mathbf{h} \, \mathrm{d}V. \tag{59}$$

Equations (58) and (59) can be written in a compact fashion as

$$\begin{bmatrix} \mathbf{M}_{aa} & 0 \\ 0 & 0 \end{bmatrix} \begin{bmatrix} \ddot{\mathbf{a}}^{t+\Delta t} \\ \ddot{\Lambda}^{t+\Delta t} \end{bmatrix} + \begin{bmatrix} \mathbf{K}_{aa} & \mathbf{K}_{a\lambda} \\ \mathbf{K}_{\lambda a} & \mathbf{K}_{\lambda\lambda} \end{bmatrix} \begin{bmatrix} \Delta \mathbf{a} \\ \Delta \Lambda \end{bmatrix} = \begin{bmatrix} \mathbf{f}^{t+\Delta t} - \mathbf{f}_{\text{int}}^t \\ \mathbf{f}_\lambda^t \end{bmatrix}, \tag{60}$$

where

$$\mathbf{M}_{aa} = \int_V \mathbf{H}^T \mathbf{R} \mathbf{H} \, \mathrm{d}V, \tag{61}$$

$$\mathbf{K}_{aa} = \int_V \mathbf{B}^T \mathbf{D}_e \mathbf{B} \, \mathrm{d}V, \tag{62}$$

$$\mathbf{K}_{a\lambda} = -\int_V \mathbf{B}^T \mathbf{D}_e \mathbf{m}' \mathbf{h}^T \, \mathrm{d}V, \tag{63}$$

$$\mathbf{K}_{\lambda a} = -\int_V \mathbf{h}(\mathbf{n}')^T \mathbf{D}_e \mathbf{B} \, \mathrm{d}V, \tag{64}$$

$$\mathbf{K}_{\lambda\lambda} = \int_V [(h' + (\mathbf{n}')^T \mathbf{D}_e \mathbf{m}') \mathbf{h} \mathbf{h}^T - \bar{c}_\eta \mathbf{h} \mathbf{p}^T] \, \mathrm{d}V, \tag{65}$$

$$\mathbf{f}^{t+\Delta t} = \int_S \mathbf{H}^T \mathbf{t}^{t+\Delta t} \, \mathrm{d}S, \tag{66}$$

$$\mathbf{f}_{\text{int}}^t = \int_V \mathbf{B}^T \boldsymbol{\sigma}^t \, \mathrm{d}V \tag{67}$$

and

$$\mathbf{f}_\lambda^t = \int_V f(\boldsymbol{\sigma}^t, \kappa^t, \nabla^2 \kappa^t) \mathbf{h} \, \mathrm{d}V. \tag{68}$$

In the Newton–Raphson iteration scheme, which is used to solve the non-linear set of algebraic equations, the values at time t are replaced by the values at time $t + \Delta t$ for the last iteration. The implicit Newmark time integration procedure has been adopted for eqn (60). Evidently the tangent stiffness matrix as defined in eqns (60)–(65) is non-symmetric because of the gradient terms and the use of a non-associative flow rule. If we assume associative plasticity ($\mathbf{m} = \mathbf{n}$ and thus $\mathbf{K}_{a\lambda} = \mathbf{K}_{\lambda a}$) the non-symmetry in eqn (65) disappears if $\bar{c}_\eta = 0$. We retrieve a symmetric operator as one would expect in classical plasticity with an associated flow rule.

For the pure rate problem the non-symmetric tangent operator defined in eqns (60)–(65) can be symmetrized. However, when we consider finite loading steps, this is not possible and symmetrization of eqn (65) therefore does not seem to offer much practical advantage. The main significance is that a formulation, which sets out from a weak formulation of the evolution equation for the inelastic state variables (de Borst and Mühlhaus, 1991, 1992), can be shown to be identical to the formulation that arises upon application of the variational principle for gradient plasticity, recently proposed by Mühlhaus and Aifantis (1991). The other advantage is that the role of the additional boundary condition on λ is elucidated. For this discussion it is sufficient to only consider the last term of eqn (65) in a rate format, or, more conveniently, eqn (44). Application of Green's theorem to this term yields:

$$\int_V \bar{c}_\eta \delta \dot{\lambda} \nabla^2 \dot{\lambda} \, \mathrm{d}V = -\int_V \bar{c}_\eta (\nabla \delta \dot{\lambda})^\mathrm{T} (\nabla \dot{\lambda}) \, \mathrm{d}V + \int_{S_\lambda} \bar{c}_\eta \delta \dot{\lambda} (\nabla \dot{\lambda})^\mathrm{T} \mathbf{n}_\lambda \, \mathrm{d}S_\lambda, \tag{69}$$

with $\mathbf{n}_\lambda$ the outward normal at the elastic–plastic boundary S_λ. From eqn (69) it follows that the condition on $\dot{\lambda}$ at the boundary of the plastically deforming part of the body must either be

$$\delta \dot{\lambda} = 0 \quad \text{or} \quad (\nabla \dot{\lambda})^\mathrm{T} \mathbf{n}_\lambda = 0. \tag{70}$$

Equation (70$_1$) is automatically satisfied at each point of the (internal) elastic–plastic boundary in the interior of the body. When the spread of the plastic zone extends to an external boundary of the body either of conditions (70) may be imposed.

With eqn (69) and assuming that the appropriate boundary conditions are satisfied $\mathbf{K}_{\lambda\lambda}$ can be rewritten as

$$\mathbf{K}_{\lambda\lambda} = \int_V [(h + \mathbf{n}^\mathrm{T} \mathbf{D}_e \mathbf{n}) \mathbf{h} \mathbf{h}^\mathrm{T} + \bar{c}_\eta \mathbf{q} \mathbf{q}^\mathrm{T}] \, \mathrm{d}V, \tag{71}$$

where

$$\mathbf{q} = [\nabla h_1, \dots, \nabla h_n]^\mathrm{T}. \tag{72}$$

Comparing eqn (60) with $\mathbf{M}_{aa}$, $\mathbf{K}_{aa}$, $\mathbf{K}_{a\lambda}$, $\mathbf{K}_{\lambda a}$ and $\mathbf{K}_{\lambda\lambda}$ as defined by eqns (61), (62), (63), (64) and (71), with the tangent stiffness operator that follows from the variational principle of Mühlhaus and Aifantis (1991), shows that both formulations yield the same result for infinitesimally small load increments. When finitely sized loading steps are used this is no longer the case and the non-symmetric definition of eqn (65) must be utilized to obtain proper convergence characteristics in an incremental-iterative procedure.

5. NUMERICAL ANALYSES

To investigate the dispersive character of the gradient-dependent model and the performance with respect to mesh refinement dynamic analyses have been carried out for a
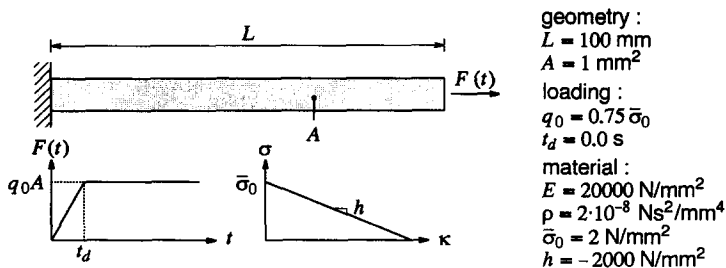
Fig. 3. One-dimensional bar problem in tension.

one-dimensional bar in tension and an impact biaxial test. The calculations have been carried out with the unconditionally stable Newmark time integration scheme (Hughes, 1987). For the time step we take $\Delta t = 5 \cdot 10^{-7}$ s for the bar problem and $\Delta t = 1.5 \cdot 10^{-6}$ s for the biaxial test. A consistent mass matrix has been used in all analyses with the gradient model.

5.1. One-dimensional bar problem in tension

First, we have investigated the gradient model by means of the one-dimensional bar problem in pure tension. The geometrical, material and loading data for the bar have been given in Fig. 3. We use a softening plasticity model according to the Rankine yield function [eqn (17)]. The extra gradient constant employed is $\bar{c}_\eta = 50,000$ N. The values for h and $\bar{c}_\eta$ imply an internal length scale parameter $l = 5$ mm [eqn (33)]. For the bar we use 20, 40, 80 and 160 line elements, respectively, with C^0-continuous shape functions for the displacement degree-of-freedom u_x and C^1-continuous shape functions for the interpolation of λ. We consider a block wave ($t_d = 0$) travelling linearly elastic through the bar until reflection occurs and the doubling in stress ($2q_0 = \frac{3}{2}\bar{\sigma}_0$) causes the initiation of the localization process. Extra boundary conditions [cf. eqn (70)] have been applied ($\partial \lambda / \partial x = 0$) at both sides of the bar.

For the gradient model a localization zone emerges with a width that converges to a finite, constant value upon mesh refinement. In Fig. 4 the strain profile is plotted for
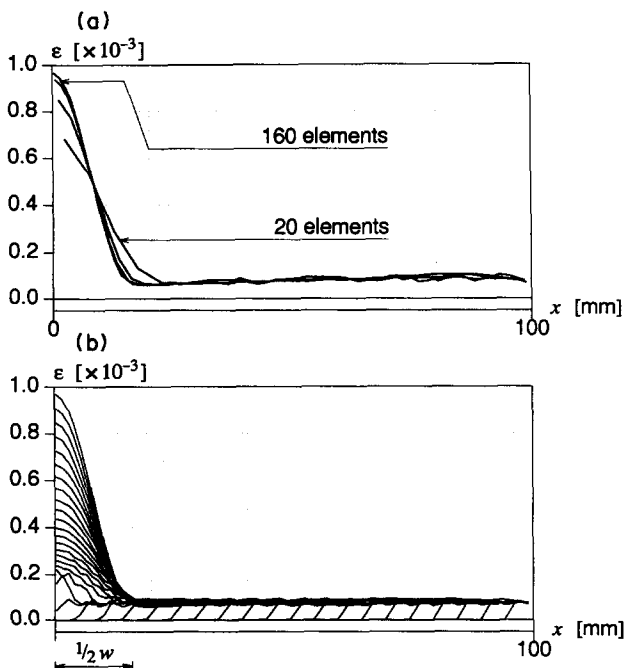

Fig. 4. Gradient-dependent model (Rankine): (a) Strain localization along the bar at $t = 0.2 \cdot 10^{-3}$ s; (b) Development of the localization band (160 elements).

different meshes to demonstrate the convergence of the solution to a finite width of the localization zone. The coarser meshes with 20 and 40 elements still deviate somewhat but the fine meshes give almost identical results. In the same figure the development of the localization band has been plotted at several time steps. First, the width of the zone increases after reflection but later, the speed of extension of the zone vanishes and a localization band of constant width arises ($\frac{1}{2}w \approx 16$ mm). Due to material damping the higher-order waves are attenuated. Owing to dispersion and material damping the shape of the loading wave changes into a first-order harmonic wave with velocity c_f equal to zero. This corresponds to a wave number $k = 0.2$ mm^{-1} and a harmonic wave length $\lambda = 2\pi l = 31.4$ mm [cf. eqns (32) and (33)]. So, the numerical localization band width w equals the first order wave length λ belonging to a phase velocity $c_f = 0$ m s^{-1} under the condition that the localization band has developed completely. The localization zone is represented by a stationary harmonic wave. In Fig. 5 it is shown that mesh independence is not only obtained for the width of the localization zone but also for the wave reflection patterns and the energy consumption. The stress profiles [Fig. 5(a)] are a superposition of the loading wave travelling to the left and the reflected wave travelling to the right. The patterns are more or less identical for the four meshes and it appears that wave reflection in a gradient-dependent bar is not determined by the number of elements. In Fig. 5(b) we observe mesh objectivity with respect to the consumption of energy U in the bar. For the gradient model, in contrast to the classical modelling, the localization zone converges to a non-zero width and to physically realistic responses for the wave reflection on the zone and the energy consumption in the zone.

The internal length scale parameter of the gradient model has been varied by taking $l = 2.5$ mm, $l = 5.0$ mm and $l = 7.5$ mm. The results in Fig. 6 prove the analytical equation for the localization band width (for this problem: $\frac{1}{2}w = \pi l$). Applying $\dot{\lambda} = 0$ as boundary condition at both sides of the bar instead of $\partial \dot{\lambda}/\partial x = 0$ affects the localization process. In Fig. 7 it is shown that the localization band develops over the total zone $w = 2\pi l$ because the plastic strain is kept zero at $x = 0$. A new stage in the localization process is entered when in some part of the localization zone the strength contribution due to local softening has vanished, so that the load-carrying capacity is only due to gradient effects. From eqns (32) and (33) it appears that the wavelength λ then starts to increase, the wave speed becomes positive and the localization zone is no longer stationary, which in turn causes an
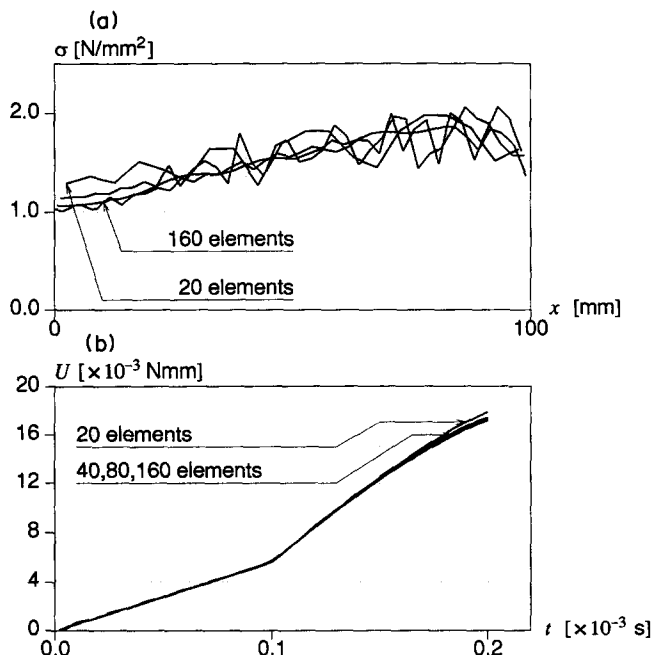

Fig. 5. Gradient-dependent model (Rankine): (a) Stress profiles along the bar at $t = 0.2 \cdot 10^{-3}$ s; (b) Energy consumption of the bar.
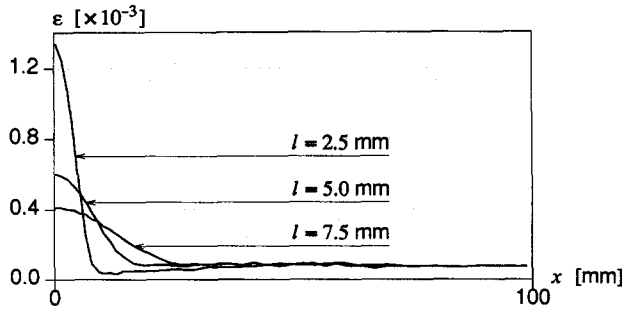
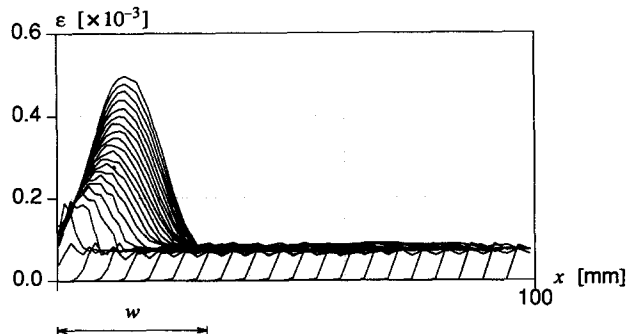Fig. 6. Variation of the length scale parameter (160 elements $-t = 0.17 \cdot 10^{-3}$ s).

Fig. 7. Application of boundary condition $\mathring{\kappa} = 0$ at both sides of the bar.

extension of the localization zone. This phenomenon is plotted in Fig. 8 for an analysis with a slightly different parameter set: $\bar{c}_\eta = 100,000$ N and $h = -4,000$ N mm^{-2} ($\kappa_u = \bar{\sigma}_0/h = 0.5 \cdot 10^{-3}$).

The width of the localization band does not depend on the loading rate. For the gradient model a higher loading rate influences the development of the localization zone but it does not affect the band width. The use of an impact loading wave with a vertical stress front ($t_d = 0$) implies a high stress rate and the presence of higher-order waves in the loading pulse. Due to dissipation of energy these higher-order waves attenuate and the vertical stress front changes into a harmonic cosine shape. When, for instance, a linearly increasing load in time ($t_d \neq 0$) is used the loading rate is smaller and higher-order waves are hardly present which cause a more gradual development of the localization zone, but the width of the localization band is not affected (Sluys et al., 1991).

5.2. Impact biaxial test

In a biaxial test a sample is subjected to a dynamic pressure load, which forces a shear band failure pattern (mode-II localization). The biaxial test problem is sketched in Fig. 9,
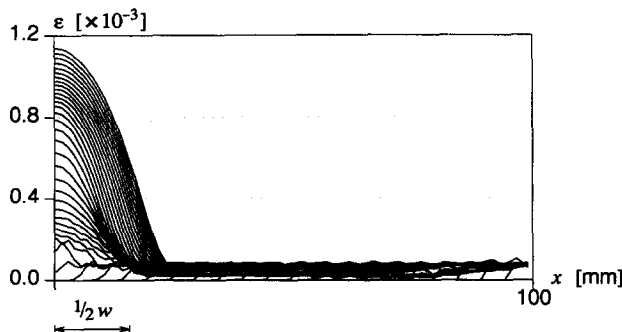

Fig. 8. Extension of the localization zone after the termination of softening.
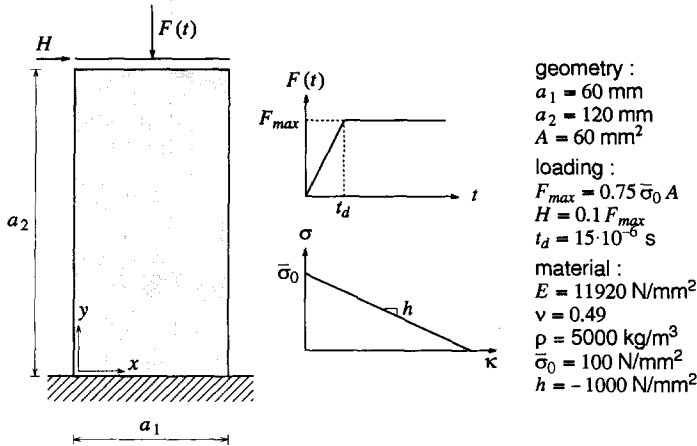
L. J. Sluys *et al.*

Fig. 9. Biaxial test.

including geometry, material and loading data. At the top of the sample a dynamic pressure load is applied. In addition a small horizontal load, which is 10% of the maximum vertical load, has been applied at the upper edge of the specimen. This load is static and forces the emergence of an asymmetric failure mode. The boundary conditions along the vertical sides are traction-free, while the bottom of the sample is rigid ($u_x = 0$ and $u_y = 0$). To ensure that all vertical displacements at the top of the sample displaced the same amount linear constraint equations have been used. As for the one-dimensional bar extra boundary conditions should be used for the sample [*cf.* eqn (70)]. At the vertical sides of the sample $\partial\lambda/\partial x$ remains zero, while at the top and bottom of the sample $\partial\lambda/\partial y$ is zero. The two-dimensional calculations for this mode-II localization problem have been carried out with a rectangular element with linear interpolation of the displacements and cubic interpolation of the plastic multiplier (Pamin and de Borst, 1992). Three finite element discretizations have been used with 72, 288 and 1,152 elements, respectively.

For a strain-softening model of the biaxial test without the incorporation of gradient effects a search algorithm should be used to determine the orientation of the shear band after which a mesh-adaptation strategy is necessary to minimize the intrinsical bias. Namely, mesh dependence for a classical continuum is not only observed for the width of the shear band upon mesh refinement but also with respect to the orientation of the mesh lines (mesh alignment). For the gradient model mesh adaptation is not necessary to exclude the spurious influence of the mesh lines. By considering the plane-strain and plane-stress condition for a von Mises type material and the plane-strain condition for a Drucker–Prager material the direction of propagation of the shear band complies with the analytically predicted direction and is not influenced by the mesh lines.

The longitudinal pressure wave propagates in a linear-elastic manner through the specimen. After reflection at the lower boundary the returning wave causes softening over the total width of the specimen. The specimen starts to bulge for a short time after reflection. Next, a gradual development of the shear band occurs and all deformation is trapped in the shear band.

Biaxial test with von Mises material (plane-strain). For the analysis with the von Mises plasticity model the material data from Fig. 9 have been used. The additional constant employed is $\bar{c}_\eta = 6{,}250$ N. With a softening modulus $h = -1{,}000$ N mm^{-2} we obtain for the length scale parameter $l = 2.5$ mm [eqn (33)].

In Fig. 10 the displacement patterns are plotted with the corresponding contour plots of the equivalent plastic strains. The inclination angle of the shear band is 45° and the width of the band is constant for the three meshes. We obtain a unique solution for the properties of the localization band. Due to dispersion and material damping the shear band transforms into a stationary harmonic wave. This can be seen from a plot of the cosine-shaped
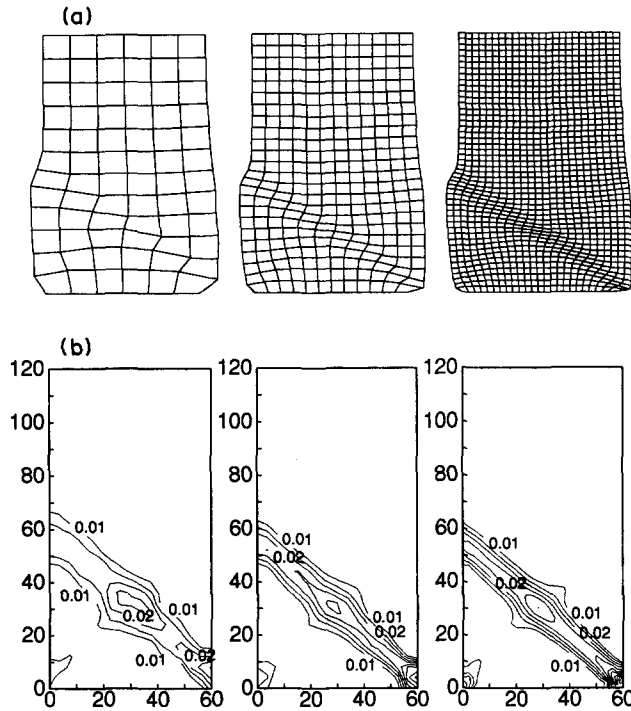
(a)

(b)

Fig. 10. Gradient model (von Mises) with plane-strain elements: (a) Total displacement patterns $(t = 0.165 \cdot 10^{-3}$ s); (b) Contour plots of the equivalent plastic strains.

equivalent plastic strains in a vertical cross-section of the sample in Fig. 11. A comparison of the consumption of energy for the meshes in Fig. 12 demonstrates the insensitiveness of the solution for the finite element discretization.

Biaxial test with von Mises material (plane-stress). The problem has also been analysed for a plane-stress condition. The parameter set is modified by taking the gradient constant $\bar{c}_\eta = 2,500$ N and the softening modulus $h = -400$ N mm^{-2}. These values result in the same length scale parameter $l = 2.5$ mm. It is important to demonstrate that the inclination angle of the shear band can vary without being influenced by the mesh lines. The analytical prediction of the inclination angle $\Theta = 35.3°$ (Sluys, 1992) comes out nicely. This is demonstrated by means of a plot of the displacements and the equivalent plastic strains in Fig. 13. Also, the solution for the width of the localization zone remains finite upon mesh refinement for the plane-stress case.

Biaxial test with Drucker–Prager material (plane-strain). The performance of the gradient model in combination with a Drucker–Prager yield criterion has been investigated for a specimen of which the configuration has been changed somewhat with respect to the
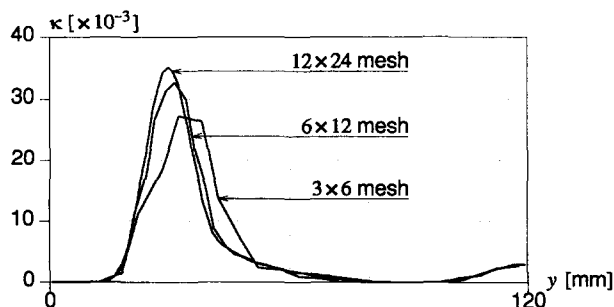

Fig. 11. Equivalent plastic strains κ in centre section ($x = 30$ mm) of the sample ($t = 0.165 \cdot 10^{-3}$ s).
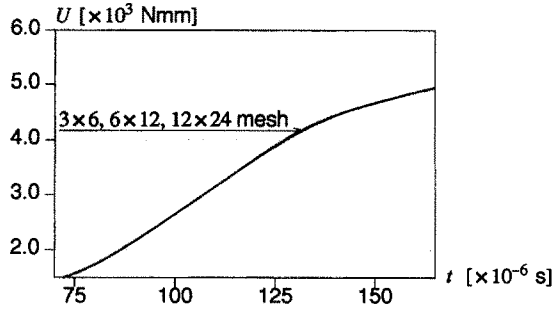
Fig. 12. Energy consumption in the sample.

specimen in Fig. 9. We consider a quadrant of a specimen and therefore the horizontal displacement is maintained at zero at the left vertical side ($u_x = 0$, $u_y \neq 0$) and the bottom of the sample is rigid and smooth ($u_x \neq 0$, $u_y = 0$). Furthermore, a longer specimen has been selected so as to admit the emergence of a shear band which now runs steeper (according to the analytical solution). The horizontal force is omitted because asymmetry in the boundary conditions already forces an asymmetric failure pattern. The data set now reads (*cf.* Fig. 9): length $a_2 = 180$ mm, pressure load $F_{max} = 150$ kN, Young's modulus $E = 2,400$ N mm^{-2}, Poisson's ratio $v = 0.2$ and density $\rho = 1,250$ kg m^{-3}. For the Drucker–Prager model the following parameters have been chosen: $\alpha = 1.2$, $\bar{\sigma}_0 = 2.08$ N mm^{-2} and a non-associative flow rule (plastically volume-preserving) is used. The cohesion parameter $\bar{\sigma}$ is linearly dependent on the equivalent plastic strain with an ultimate strain $\kappa_u = 0.005$. For the gradient model we take $\bar{c}_\eta = 1,800$ N and if we set h in eqn (33) equal to $d\bar{\sigma}/d\kappa$ we obtain a length scale parameter $l = 3.0$ mm. The additional boundary conditions listed in the analysis for the von Mises model have also been used for this analysis.

The results of the plane-strain analysis after one cycle ($t = 0.24 \cdot 10^{-3}$ s) of the pressure wave have been plotted in Fig. 14. Again, we observe that refinement of the mesh has no influence on the size of the shear band. The shear band is initiated at the bottom left corner
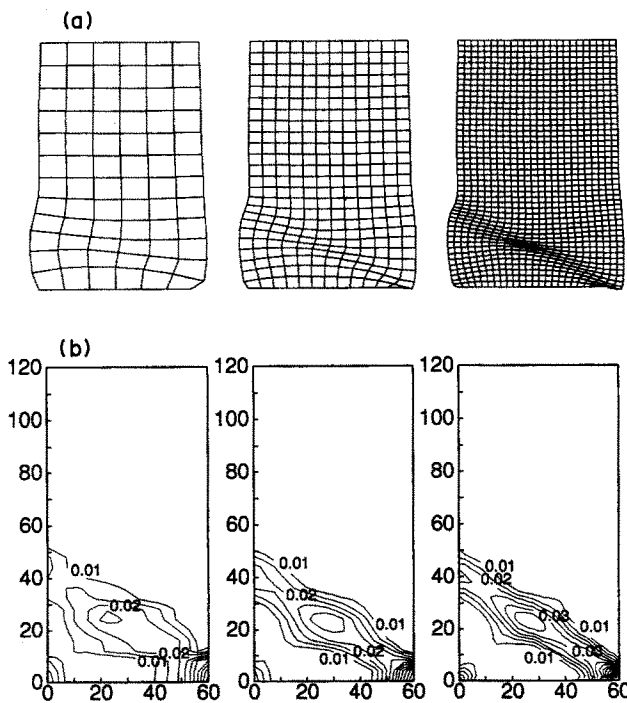

Fig. 13. Gradient model (von Mises) with plane-stress elements: (a) Total displacement patterns ($t = 0.165 \cdot 10^{-3}$ s); (b) Contour plots of the equivalent plastic strains.
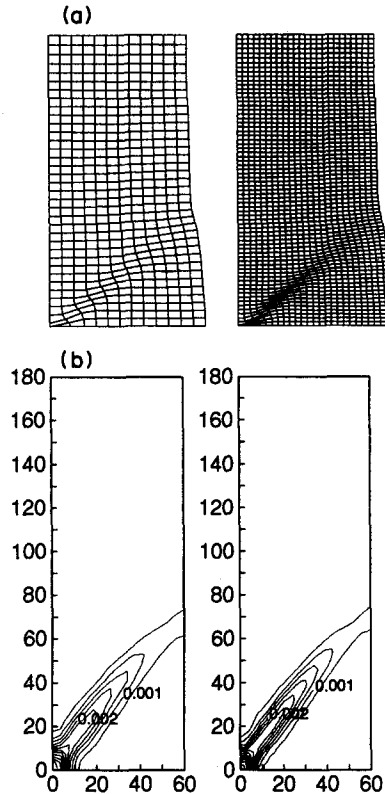
Fig. 14. Gradient model (Drucker–Prager) with plane-strain elements: (a) Total displacement patterns ($t = 0.24 \cdot 10^{-3}$ s); (b) Contour plots of the equivalent plastic strains.

of the specimen with an inclination angle $\Theta \approx 50°$, while analytically it was obtained that $\Theta = 48.4°$ (Sluys, 1992). We observe a clear mismatch in orientation between the shear band in the interior and on the boundary of the specimen. Needleman and Ortiz (1991) have explained this phenomenon by means of an analytical treatment of the interaction between the shear band in the interior of the body and a stationary Rayleigh wave at the free boundary. A remarkable result is obtained if we take the internal friction angle $\alpha = 0.77$. Figure 15 shows that the shear band now starts at the bottom right corner of the specimen. This change of orientation is due to the fact that a different stress state in the bottom corners of the specimen in combination with a different angle of internal friction leads to a different location of the critical state which drives the propagation of the shear band (Sluys, 1992). The numerically obtained inclination angle for $\alpha = 0.77$ equals $\Theta \approx 49°$, which is in reasonable accordance with the analytical value $\Theta = 47.0°$.

6. CONCLUDING REMARKS

The ill-posedness of the set of partial differential equations, the absence of an internal length scale and the inability to reproduce dispersive waves are the basic deficiencies of the use of strain-softening models in a standard, rate-independent continuum. Localization of deformation then necessarily occurs in a line (in a two-dimensional continuum) or in a plane (in a three-dimensional continuum) and coincides with loss of hyperbolicity of the initial value problem. The ensuing loss of well-posedness results in a bizarre mesh sensitivity in numerical computations.

In this paper the gradient approach has been followed to overcome the above-mentioned deficiencies. The second gradient of the equivalent plastic strain has been incorporated in the yield function. In the gradient model the yield function has been satisfied in a weak sense which results in a formulation in which the plastic multiplier is treated as an independent variable. For one-dimensional wave propagation in the gradient-dependent
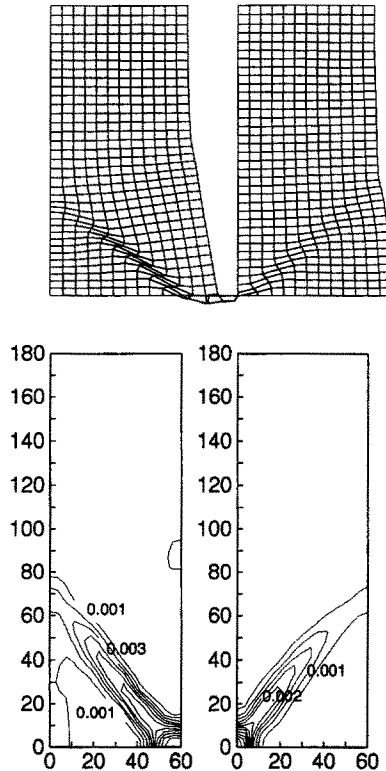
Fig. 15. Gradient model (Drucker–Prager) with plane-strain elements using friction coefficient $\alpha = 0.77$ (left) and $\alpha = 1.2$ (right). Note that the displacements have been multiplied by a factor 150.

medium the well-posedness of the initial value problem has been demonstrated and the presence of an internal length scale has been shown to follow from an analysis of dispersive waves. The dispersive waves with real wave speeds cause the extension of the localization zone and the transformation of the strain profile in the localization zone.

The numerical analyses show that the solution converges to a finite width of the localization zone that agrees with the analytical value and to mesh-insensitive results with respect to wave reflection and energy consumption. These results have been obtained for mode-I and for mode-II localization problems under impact loading. For the latter case (a shear band analysis in a biaxial test) it has been demonstrated that not only the width of the band converges to a finite value but also that the orientation of the band is not influenced by the direction of the mesh lines (alignment issue).

REFERENCES

Aifantis, E. C. (1984). On the microstructural original of certain inelastic models. *J. Engng Mater. Technol.* **106**, 326–334.
Aifantis, E. C. (1992). On the role of gradients in the localization of deformation and fracture. *Int. J. Engng Sci.* **30**(10), 1279–1299.
Bažant, Z. P., Belytschko, T. B. and Chang, T.-P. (1984). Continuum theory for strain-softening. *ASCE J. Engng Mech.* **110**, 1666–1692.
de Borst, R. and Feenstra, P. H. (1990). Studies in anisotropic plasticity with reference to the Hill criterion. *Int. J. Num. Meth. Engng* **29**, 315–336.
de Borst, R. and Mühlhaus, H.-B. (1991). Computational strategies for gradient continuum models with a view to localisation of deformation. In *Proc. Int. Conf. on Nonlinear Engng Comp.* (Edited by N. Bićanić, P. Marović, D. R. J. Owen, V. Jović and A. Mihanović), pp. 239–260. Pineridge Press, Swansea.

de Borst, R. and Mühlhaus, H.-B. (1992). Gradient-dependent plasticity: Formulation and algorithmic aspects. *Int. J. Num. Meth. Engng* **35**, 521–539.

Hughes, T. J. R. (1987). The finite element method—linear static and dynamic finite element analysis. Prentice-Hall, New Jersey.

Lasry, D. and Belytschko, T. B. (1988). Localization limiters in transient problems. *Int. J. Solids Structures* **24**, 581–597.

Mühlhaus, H.-B. and Aifantis, E. C. (1991). A variational principle for gradient plasticity. *Int. J. Solids Structures* **28**, 845–858.

Needleman, A. and Ortiz, M. (1991). Effect of boundaries and interfaces on shear-band localization. *Int. J. Solids Structures* **28**, 859–878.

Ortiz, M. and Simo, J. (1986). An analysis of a new class of integration algorithms for elastoplastic constitutive equations. *Int. J. Num. Meth. Engng* **23**, 353–366.

Pamin, J. and de Borst, R. (1992). A rectangular element for gradient plasticity. In *Proc. Conf. on Computational Plasticity, Fundamentals and Applications, Part II* (Edited by D. R. J. Owen, E. Oñate and E. Hinton), pp. 2009–2020. Pineridge Press, Swansea.

Pijaudier-Cabot, G. and Bažant, Z. P. (1987). Nonlocal damage theory. *ASCE J. Engng Mech.* **113**, 1512–1533.

Schreyer, H. L. and Chen, Z. (1986). One-dimensional softening with localization. *J. Appl. Mech.* **53**, 791–797.

Simo, J. (1989). Strain-softening and dissipation: a unification of approaches. In *Cracking and Damage: Strain Localization and Size Effect* (Edited by J. Mazars and Z. P. Bažant), pp. 440–461. Elsevier, London-New York.

Sluys, L. J. (1992). Wave propagation, localisation and dispersion in softening solids. Dissertation, Delft University of Technology, Delft.

Sluys, L. J., de Borst, R. and Mühlhaus, H.-B. (1991). Wave propagation and localisation in a gradient-dependent elastic–plastic solid. In *Proc. Int. Conf. on Nonlinear Engng Comp.* (Edited by N. Bićanić, P. Marović, D. R. J. Owen, V. Jović and A. Mihanović), pp. 287–297. Pineridge Press, Swansea.

Whitham, G. B. (1974). Linear and nonlinear waves. John Wiley and Sons, New York-London-Sydney-Toronto.

Zbib, H. M. and Aifantis, E. C. (1988). On the localization and postlocalization behavior of plastic deformation, I, II, III. *Res. Mech.* **23**, 261–277, 279–292, 293–305.